25th ABCM International Congress of Mechanical Engineering
October 20-25, 2019, Uberlândia, MG, Brazil

COBEM2019-1674
A TRANSIENT MODEL OF A TWO-PHASE LOOP THERMOSIPHON BASED ON MICROCHANNELS

André Felipe Massaro Pucciarelli
Gherhardt Ribatski

Heat Transfer Research Group, Department of Mechanical Engineering, Escola de Engenharia de São Carlos, University of São Paulo – Av. Trabalhador São Carlense, 400 – Parque Arnold Schimidt
andre.pucciarelli22@gmail.com
ribatski@sc.usp.br

Abstract. *This paper presents a model to evaluate the performance of a two-phase thermosiphon loop based on microchannels. The model was developed for steady state and transient regimes and is based on the functional iteration method. The model provides as results the mass flow rate, temperature distribution, pressure drop, fluid inventory and the overall thermal resistance of the thermosiphon during transient operation. The model predicts the increase of the mass flow rate and the footprint temperature of the evaporator, and decreasing of the overall thermal resistance with increase the heating power.*
Keywords: *thermosiphon, transient simulation, microchannels, thermal resistance*

1. INTRODUCTION

According to Kooney (2011), the energy consumption of data centers is rapidly increasing and is responsible for 1.1 to 1.5% of the world electricity consumption. Garrity *et al.* (2007) show that more than 50% of the heat generated in high density fuel cells must be removed to prevent dry out and local degradation of the membrane. Another aspect concerning energy consumption of fuel cells highlighted by Berning *et al.* (2003) and Wetton *et al.* (2004) is the fact that increasing the pumping power to drive the coolant fluid implies on reducing the overall net power output of the fuel cells. The augmentation of the overall power consumption is also observed by increasing the cooling fluid pumping power in data centers, as pointed out by Marcinichen *et al.* (2016).

Recent studies shown that two-phase loop thermosiphons may provide a satisfactory solution for the problems quoted above. They are pumpless gravity-driven devices composed of the following four main elements: an evaporator, a condenser and two adiabatic tubes (a riser and a downcomer). The heat is removed from its source through the evaporator, where the fluid boils. The riser is the medium for transporting the working fluid to the condenser, where the heat is rejected. Then, the fluid is driven back to the evaporator by gravitational effects through the downcomer, closing the loop. In these devices, the fluid flow along the loop is sustained by the height difference between the evaporator and the condenser together with the density difference between the fluids in the downcomer and in the riser.

The mass flow rate along the two-phase thermosiphon loop depends on the heat input in the evaporator. Khodabandeh (2005) and Franco and Fellipeschi (2013) observed two operational regimes for the thermosiphon: (i) *the gravity dominant regime*, when the mass flow rate increases with increasing the heat input; and (ii) *the friction dominant regime*, when the condenser is not capable of compensating the heat input at the evaporator, increasing the pressure drop at the condenser and at the downcomer, decreasing the mass flow rate.

Recently, Zhang *et al.* (2017) and Marcinichen *et al.* (2016) developed new models to evaluate the performance of two-phase loop thermosiphons. Both methods are based on the principle that a thermosiphon operates with the static pressure gain becoming equals to the pressure drop of the flow along the thermosiphon components. This condition was first set by Chexal (1973) based on his study about instabilities in natural circulation loops.

The model described in this paper is based on a functional iteration method for the prediction of the performance of a two-phase loop thermosiphon composed of microchannels.

2. METHOD DESCRIPTION

As stated above, the height and density difference between evaporator and condenser are responsible for sustain the flow. The equation for the driving pressure is given as follows:

$$\Delta p_{driving} = gH\left(\rho_l - \rho_{2\phi}\right) \tag{1}$$

where: g is the gravitational acceleration, H is the difference of height between the evaporator and the condenser and ρ_l and $\rho_{2\Phi}$ are the density in the downcomer and in the riser, respectively.

It is necessary that the driving pressure overcomes the pressure drop along the components of the loop in order to trigger the thermosiphon operation. Therefore, by adopting the hypothesis of Chexal (1973) the operational condition is set as follows:

$$\Delta p_{gain} - \Delta p_{drop} \simeq 0 \tag{2}$$

The model developed in the present paper is based on the discretization of the thermosiphon components and on the mass, momentum and energy balances over each one of them. The model is valid for gravity and friction dominant regimes and was developed for a thermosiphon prototype available at the Heat Transfer Research Group. On the following sections, the modelling procedure is detailed.

2.1 Model Description

A schematic drawing of the simulated two-phase thermosiphon loop is shown in Fig. 1.

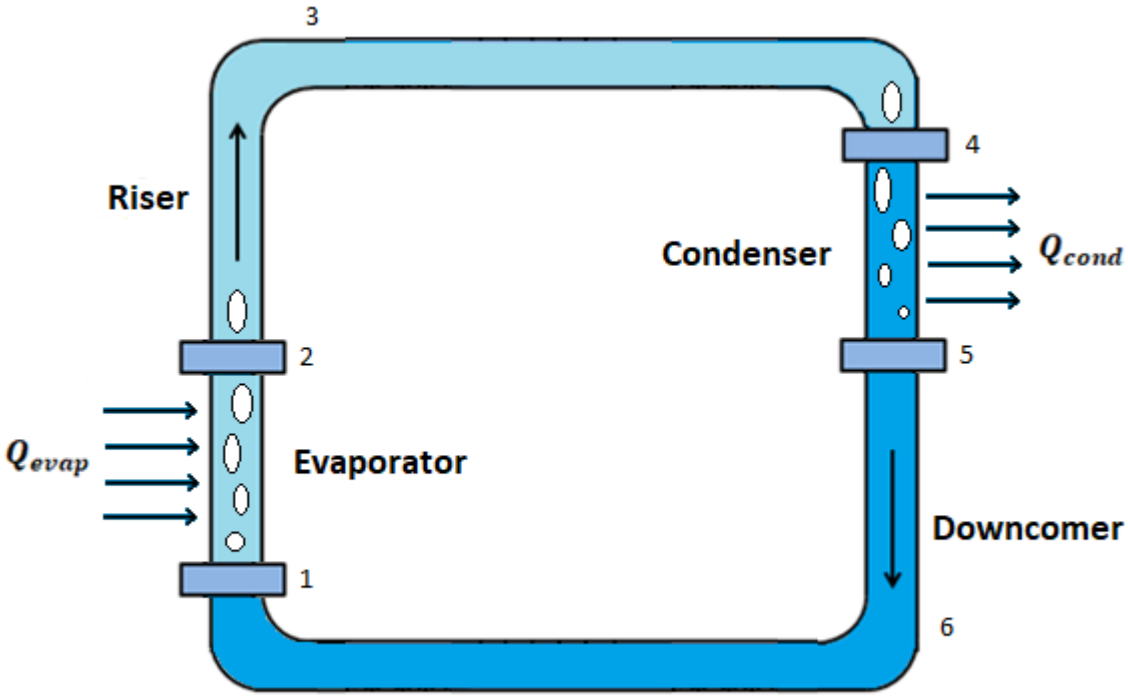

Figure 1: Schematic drawing of the two-phase thermosiphon loop.

At point 1, the heated section of the evaporator is composed of 14 rectangular vertical microchannels with cross section of 1.5 x 2.0 mm and length of 50 mm. The two-phase flow reaches the riser at point 2. The riser and the evaporator are composed of continuous microchannels with total length of 191.5 mm. At point 3, the riser is followed by the superior plenum, which is composed of a rectangular horizontal single channel with cross section of 20 x 60 mm and length of 141.5 mm. At point 4, the two-phase flow reaches the cooling section of the condenser, which is also composed by 14 rectangular microchannels with 1.5 x 2.0 mm and length of 50 mm. The height difference between points 2 and 5 is 38 mm. At point 5, the liquid flow reaches the downcomer, which is composed by a square single channel with 20 x 20 mm and length of 50 mm. At point 6, the inferior plenum is composed by a rectangular single channel with the same dimensions as the superior plenum.

The dimensions of the components of the thermosiphon are given in Table 1.

Table 1: Geometrical parameter of the two-phase loop thermosiphon

Characteristic	Evaporator	Condenser
Cross section geometry	Rectangular	Rectangular

Number of microchannels	14	14
Length x depth [mm²]	2.0 x 1.5	2.0 x 1.5
Heated/cooled length [mm]	50	50
Height difference [mm]	38	
Material	Aluminum	

The following hypothesis and approximations were assumed for the model development: at each instant, similar mass flow rates are assumed along the loop; the velocity profile is uniform; unidimensional heat conduction in the evaporator and condenser walls; fluid thermal properties constant along each discrete element; fins of the evaporator and condenser with adiabatic edge; negligible pressure drop at the restrictions, elbows and channel enlargements and uniform surface temperature along the footprint surface of the condenser.

The local pressure of each discrete element of the thermosyphon was calculated as follows:

$$p_{i+1} = p_i - \Delta p_{ac.} - \Delta p_{fric.} - \Delta p_{grav.} \tag{3}$$

The fluid properties were calculated locally for each element using the REFPROP.

Besides the geometrical parameters, the input data of the simulations are the following: heat input on the evaporator, evaporation temperature at the bottom of the riser and fluid subcooling at the evaporator inlet. An initial vapor quality value is also guessed. Mass flow rate and vapor quality at the end of the evaporator were estimated.

At steady state analysis, momentum and energy balances were applied for each element, starting at the bottom of the riser. In this calculus, prediction methods for frictional pressure drop, void fraction and heat transfer coefficient from literature were adopted.

The convergence of the calculus was evaluated at the end of the evaporator. The convergence was assured when the difference between the pressure gain and pressure drop becomes lower than 10^{-9} Pa. If convergence is not attained, a new vapor quality at the end of evaporator is assumed, given as follow:

$$x_{j+1} = x_j \frac{\Delta p_{drop}}{\Delta p_{gain}} \tag{4}$$

Then, new mass flow rate and inlet subcooling are estimated based on an energy balance along the evaporator assuming the new vapor quality. The new subcooling temperature is calculated to compensate the new vapor quality with the same heat input.

The analysis for transient regime is performed when the heat flux in the evaporator is varied from a steady state condition. Initially, the steady state analysis is performed considering the initial heat input. In the next step, energy and momentum balances are applied to each discretized element at each time step. The transient energy conservation equation is given as:

$$\frac{\partial(\rho_{lv} i)}{\partial t} = -\frac{\partial(\rho_{lv}.u.i)}{\partial z} + \frac{P.Q}{A} \tag{5}$$

Steady state at a specific time step is reached when the left term of Eq. 5 is equal or less than 10^{-5} W, when these criteria is satisfied, the mass flow rate for the next time step is given by the equation below proposed by Marcinichen *et al.* (2016) as:

$$\frac{d\dot{m}}{dt} = K(p_{t+dt} - p_t) \tag{6}$$

The term 'K' is a gain used to reduce the simulation time and to guarantee the convergence of the equation system. In the present study, its value was set equal to 0.005 kg/s.Pa.

In the model, each component of the thermosiphon was composed of 20 discrete elements. This number of elements assured the convergence of the simulations as displayed in Fig. 2.

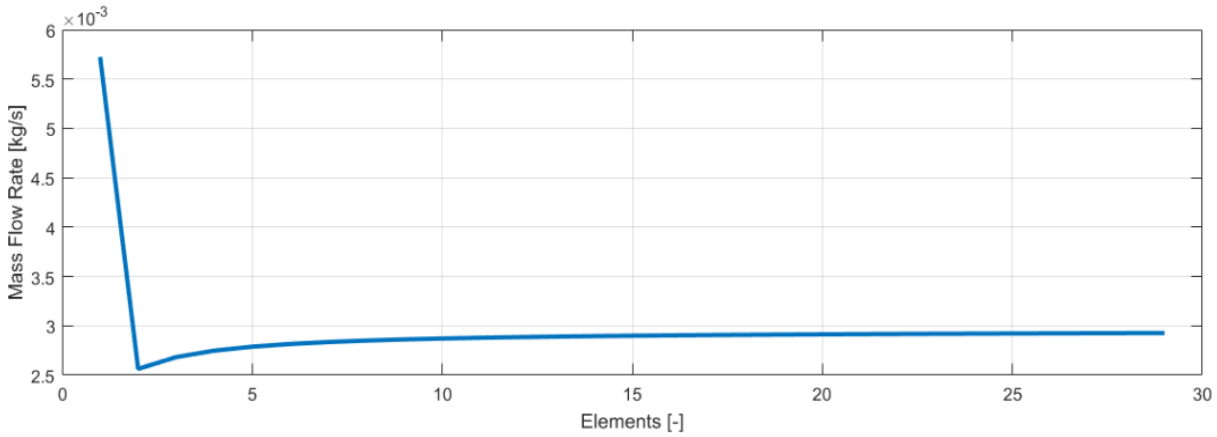

Figure 2: Convergence of the simulation.

2.2 Prediction Methods for Heat Transfer, Pressure Drop and Void Fraction

The prediction methods adopted in the model were selected taken into account the geometry of the components and the flow orientation along the thermosiphon. Care was exercised in order to select prediction methods based on experimental conditions close to those occurring along the thermosiphon.

Table 2: Prediction methods adopted in the simulation.

Type	Prediction Methods
Void fraction – vertical	Kanizawa and Ribatski. (2016)
Two-phase friction pressure drop	Sempértegui – Tapia and Ribatski (2017)
Single-phase friction pressure drop	Blasius (1913)
Single-phase heat transfer coefficient	London e Shah (1978)
Condenser two-phase heat transfer coefficient	Park *et al.* (2011)
Evaporator two-phase heat transfer coefficient	Kanizawa *et al.* (2016)

The prediction method of Kanizawa and Ribatski (2016) for void fraction was chosen due to the experimental database used to adjust its empirical constants that includes results for saturated vertical flows, mass velocities from 70 to 800 kg/s.m² and channels with internal diameters from 0.5 to 13.8 mm. In a similar manner, the method for frictional pressure drop proposed by Sempértegui – Tápia and Ribatski (2017) was selected because the database used for the adjustment of its empirical coefficients covers mass velocities from 100 to 1600 kg/s.m², vapor qualities ranging from 0.05 to 0.95 and a channel with a cross section similar to the ones of the evaporator and the condenser of the thermosiphon.

For prediction of the heat transfer coefficient under single-phase conditions in the evaporator and condenser, London e Shah (1978) method for developing flow was chosen, adopting the edges of the fins as adiabatic. The heat transfer coefficient under conditions of condensation was estimated based on the method of Park *et al.* (2011). This method was developed based on data for vertical downward flow in rectangular microchannels, covering mass velocities from 50 to 260 kg/s.m² and vapor qualities from 0.0 to 1.0. The heat transfer coefficient in the evaporator was estimated using the method of Kanizawa *et al.* (2016) developed based on experimental results for internal diameters from 0.38 to 2.6mm, heat fluxes up to 185 kW/m² and mass velocities from 49 to 2200 kg/s.m².

3. RESULTS

In this section, the results of the simulations obtained for a case study are presented. The initial contition were set as presented in Table 3.

Table 3: Initial conditions inputs to the simulation.

Input	Value
Working Fluid	Ethanol
Input Pressure [kPa]	558
Power [W]	10 to 200 / 200 to 30 W.

Fig. 3 shows the variaton of the mass flow rate with time for a change in the heating power from 10 to 200 W (at 1000 s) and from from 200 to 30 W (at 4500 s) using ethanol as working fluid and a saturation pressure of 559 kPa at the evaporator outlet. Following the first disturbance, the mass flow rate initially decreases with the increase of the heat input. This behavior is associated to the increase of the vapor amount at the evaporator, impplying on extra friction. Later, with the propagation of the vapor alongthe riser, the density of the two-phase flow decreases, increasing the mass flow rate due to extra driving potential. Later, the mass flow rate stabilizes to a new value, satisffying Eq. 2. According to Marcinichen *et al.* (2014), the increase of the heat transfer due to the increase of the amount of vapor helps to increase the bouyancy effect along the riser, increasing the mass flow rate. Lamaison *et al.* (2016) obtained similar behavior increasing the power. Later, with the reduction of the power, the amount of vapor at the riser tube is reduced, reducing the bouyancy effects and, consequently, reducing the mass flow rate. Marcinichen *et al.* (2014) obtained similar results for R134a.

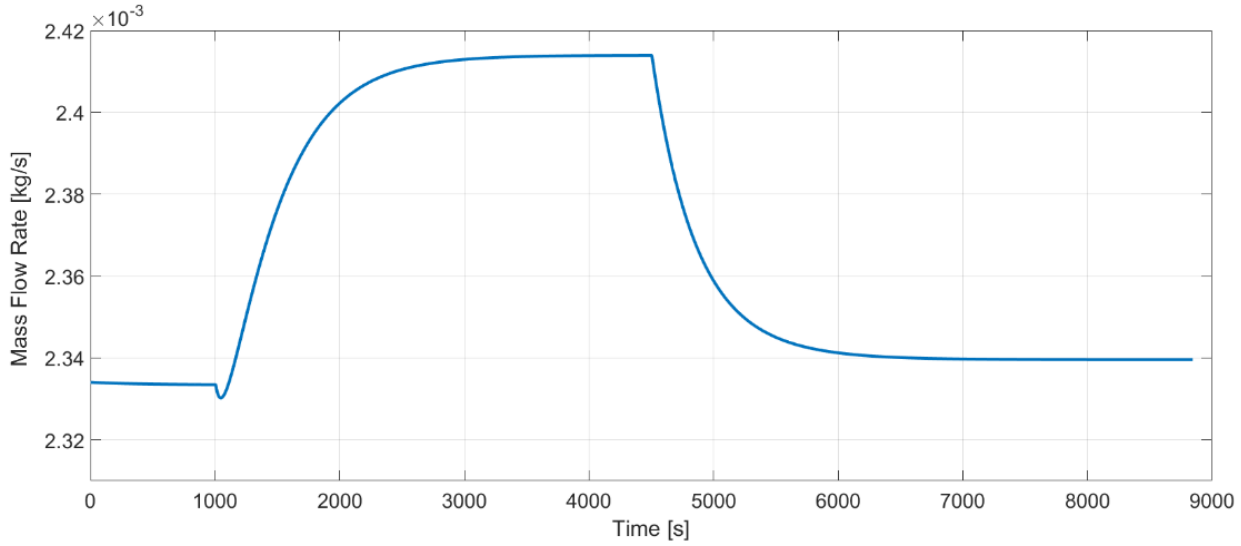

Figure 3. Variation of mass flow rate with time for ethanol.

Fig. 4 shows the variation the global thermal resistance of the two phase loop thermosiphon with the variation of the heating power. As the heating power increases from 10 to 200 W, the thermal resistance is reduced until steady state is reached at a period of 4500 s. This reduction occurs simultaneously to the increase of the mass flow rate. The sudden decrease of the thermal resistance due to the disturbance on the power might be explained due to the instantaneous boiling at the evaporator, increasing the heat transfer coefficient along its length. The condensation heat transfer coefficient also increases. The oposite behavior is observed during the reduction of the heating power at 4500 s, implying on the increase of the thermal resistance due to mainly the decrease of the boiling heat transfer coefficient.

The working fluid charge has significant effect on the loop thermal performance of the thermosiphon, as observed by Louahlia-Gualous *et al.* (2017), Chehade *et al.* (2014), Li *et al.* (2018) and Liu *et al.* (2019). According to their studies, lower filling ratios are associated with dry out at the evaporator section, providing higher values of thermal resistance, reducing the heat transfer. Higher filling ratios are associated with liquid flooding at the condenser, reducing the contact area between the vapor and the surface, increasing also the thermal resistance. Therefore, there is an optimal range of filling ratio that provides lower values of thermal resistances. Unfortunately, the present model is not capable of capture the effect of the filling ratio, as the models of Zhang *et al.* (2017).

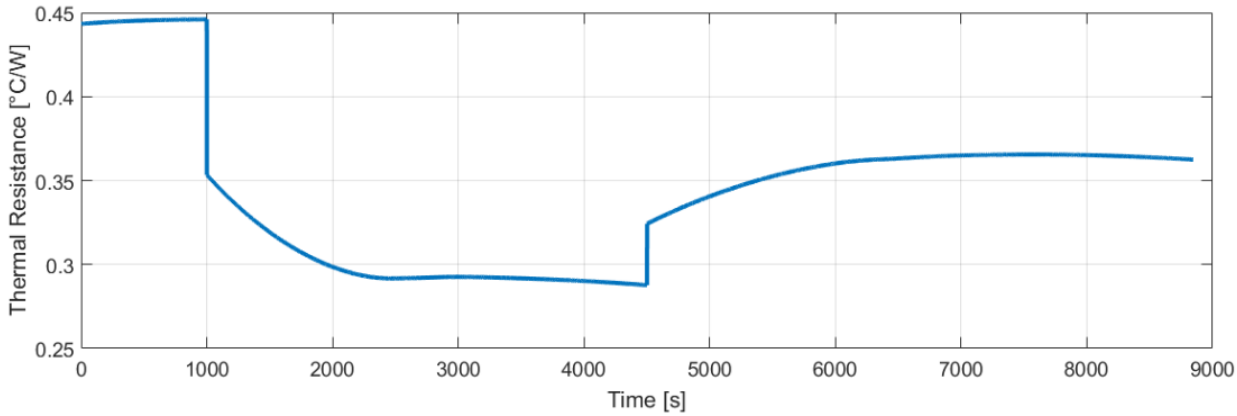

Figure 4. Variation of the thermal resistance with time for ethanol.

The behaviors displayed in Fig. 4 are similar to the ones obtained by Louahlia-Gualous *et al.* (2017) and Li *et al.* (2018), providing reduced values for thermal resistance, showing that the tested two-phase thermosiphon loop could be applied in practical uses.

According to Marcinichen *et al.* (2014), when the heating input is changed, the first effect on the thermosiphon loop is on the footprint temperature, affecting, then, the mass flow rate, vapor quality and pressure drop.

Fig. 5 show the effect of the variation of footprint temperature with time considering the power input changed considered in Figs. 3 and 4. As observed, at the first disturbance, the temperature presents a sudden increase, followed by a continuous decreasing associated to the decrease of overall thermal resistance, as dispalyed in Fig. 4. The opposite effect is observed at the second disturbance, with the reduction of power input. As expected, the temperature difference between the initial and final conditions is higher when increasing the power input from 10 to 200W (≈45oC) than when decreasing the power input from 200 W to 30 W (≈28oC). It is also observed that the peak footprint temperature obtained with 200 W is 110 °C, which might be problematic to some applications, like in refrigeration systems of chip processors.

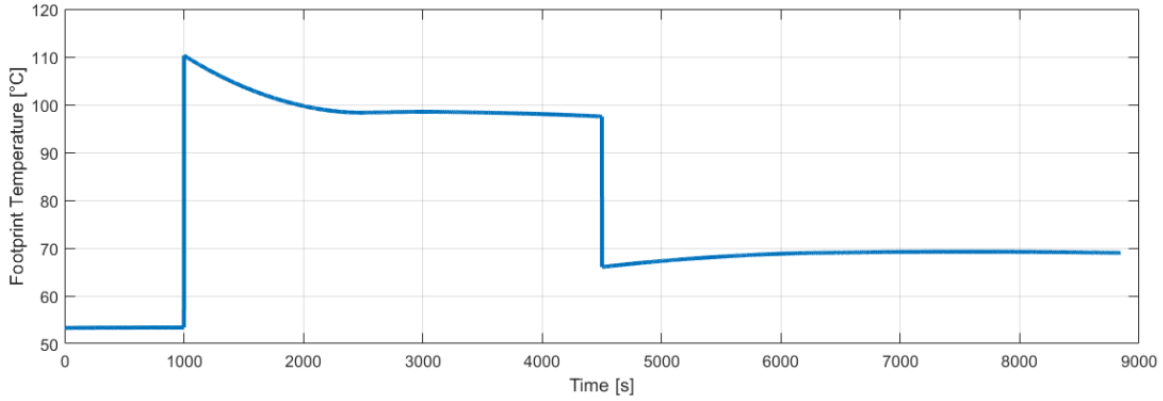

Figure 5. Footprint temperature at the evaporator section.

4. CONCLUSIONS

In this paper, a two-phase thermosiphon model is proposed. The model is based on a functional iterative method with a one-dimensional space discretization of the loop. The tests were made to predict the thermal performance of a two-phase thermosiphon available at the São Carlos Heat Transfer Group, designed for the thermal management of fuel cells. The obtained results shows that the thermosiphon might be applied in low and high heat inputs (10 and 200 W) for ethanol and the simulated results are consistent with the literature, predicting the increase of the mass flow rate and the footprint temperature of the evaporator, and decreasing of the overall thermal resistance with increase the heating power. .The model still doesn't capture the effects of the filling ratio on the thermal performance, but further analysis will be made to add those effects.

In a future work, the results obtained with those simulations will be experimentally compared with experimental results for the thermosiphon available at the Heat Transfer Research Group.

5. ACKNOWLEDGMENTS

The authors acknowledge the CNPq (National Council for Scientific and Technological Development, Brazil) for the grants given to the first author and the support to the Mechanical Engineering Graduate Program of EESC-USP given by CAPES (Coordination for the Improvement of Higher Level Personal, Brazil). The authors also acknowledge the FAPESP (São Paulo Research Foundation, Brazil) for the thematic grant under Contract Number 2011/50727-9 that provides support to this study.

6. REFERENCES

Berning, T.; Djilali, N. Parametric Study of Transport phenomena in PEM Fuel Cells using a 3D Computational model. In: ASME 2003 1st International Conference on Fuel Cell Science, Engineering and Technology. American Society of Mechanical Engineers, 2003. p. 187-194.

Chexal, V. K. Two-phase instabililties in a low pressure natural circulation loop (Doctoral dissertation, Georgia Institute of Technology), 1972.

Franco, A.; Filippeschi, S. Experimental analysis of closed loop two phase thermosiphon (CLTPT) for energy systems. Experimental thermal and fluid science, v. 51, p. 302-311, 2013.

Garrity, P.T.; Klausner, J. F.; Mei, R. A flow boiling microchannel evaporator plate for fuel cell thermal management. Heat Transfer Engineering, v. 28, n. 10, p. 877-884, 2007.

Kanizawa, F. T.; Ribatski, G. Void fraction predictive method based on the minimum kinetic energy. Journal of the Brazilian Society of Mechanical Sciences and Engineering, v. 38, n. 1, p. 209-225, 2016.

Kanizawa, F. T.; Tibiriçá, C. B.; Ribatski, G. Heat transfer during convective boiling inside microchannels. International Journal of Heat and Mass Transfer, v. 93, p. 566-583, 2016.

Khodabandeh, R.. Heat transfer in the evaporator of an advanced two-phase thermosiphon loop. International Journal of Refrigeration, v. 28, n. 2, p. 190-202, 2005.

Koomey, Jonathan. Growth in data center electricity use 2005 to 2010. A report by Analytical Press, completed at the request of The New York Times, v. 9, 2011.

Lamaison, N., Marcinichen, J. B., Ong, C. L., Thome, J. R. (2016, May). Two-phase mini-thermosiphon electronics cooling, Part 4: Application to 2U servers. In *2016 15th IEEE Intersociety Conference on Thermal and Thermomechanical Phenomena in Electronic Systems (ITherm)* (pp. 599-609). Ieee

Marcinichen, J. B., Lamaison, N., Ong, C. L., Thome, J. R. Two-phase mini-thermosiphon electronics cooling, part 2: Model and steady-state validations. In 2016 15th IEEE Intersociety Conference on Thermal and Thermomechanical Phenomena in Electronic Systems (ITherm), 2016, pp. 582-588.

Marcinichen, J. B., Szczukiewicz, S., Lamaison, N., Thome, J. R. (2014, May). Towards development of a passive datacenter cooling technology: On-server thermosiphon cooling loop under dynamic workload. In *Fourteenth Intersociety Conference on Thermal and Thermomechanical Phenomena in Electronic Systems (ITherm)* (pp. 1027-1037). IEEE.

Sempértegui-tapia, D. F.; Ribatski, G. Two-phase frictional pressure drop in horizontal micro-scale channels: experimental data analysis and prediction method development. International Journal of Refrigeration, v. 79, p. 143-163, 2017.

Shah, R. K.; London, A. L.. Laminar flow forced convection in ducts: a source book for compact heat exchanger analytical data. Academic press, 2014.

Wetton, B.; Promislow, K.; Caglar, A. A simple thermal model of PEM fuel cell stacks. In: ASME 2004 2nd International Conference on Fuel Cell Science, Engineering and Technology. American Society of Mechanical Engineers, 2004. p. 151-155.

Zhang, H., Shao, S., Jin, T., Tian, C. Numerical investigation of a CO2 loop thermosiphon in an integrated air conditioning system for free cooling of data centers. Applied Thermal Engineering, 126, 1134-1140, 2017.

7. RESPONSIBILITY NOTICE

The authors are the only responsible for the printed material included in this paper.